frontiers | Frontiers in Materials

ORIGINAL RESEARCH
published: 11 April 2022
doi: 10.3389/fmats.2022.850610

Simulation Study on Internal Short Circuits in a Li-Ion Battery Depending on the Sizes, Quantities, and Locations of Li Dendrites

Suhwan Kim[1†], Jihun Song[1†], Hyobin Lee[1], Seungwon Jung[1], Joonam Park[2], Hongkyung Lee[1,2] and Yong Min Lee[1,2*]*

[1]Department of Energy Science and Engineering, Daegu Gyeongbuk Institute of Science and Technology (DGIST), Daegu, South Korea, [2]Energy Science and Engineering Research Center, Daegu Gyeongbuk Institute of Science and Technology (DGIST), Daegu, South Korea

OPEN ACCESS

Edited by:
Wolfgang Wenzel, Karlsruhe Institute of Technology (KIT), Germany

Reviewed by:
Maria Helena Braga, University of Porto, Portugal
Rachel Carter, Naval Research Laboratory, United States

***Correspondence:**
Hongkyung Lee
hongkyung.lee@dgist.ac.kr
Yong Min Lee
yongmin.lee@dgist.ac.kr

[†]*These authors have contributed equally to this work*

Specialty section:
This article was submitted to Computational Materials Science, a section of the journal Frontiers in Materials

Received: *07 January 2022*
Accepted: *14 March 2022*
Published: *11 April 2022*

Citation:
Kim S, Song J, Lee H, Jung S, Park J, Lee H and Lee YM (2022) Simulation Study on Internal Short Circuits in a Li-Ion Battery Depending on the Sizes, Quantities, and Locations of Li Dendrites. Front. Mater. 9:850610. doi: 10.3389/fmats.2022.850610

The internal short circuit caused by the Li dendrite is well known to be a major cause for fire or explosion accidents involving state-of-the-art lithium-ion batteries (LIBs). However, post-mortem analysis cannot identify the most probable cause, which is initially embedded in the cell, because the original structure of the cell totally collapses after the accident. Thus, multiphysics modeling and simulation must be an effective solution to investigate the effect of a specific cause in a variety of conditions. Herein, we reported an electrochemical-thermal model to simulate the internal short circuit depending on Li dendrite's sizes (1, 3, 5, 7, and 9 μm), quantities (1–9), relative locations (0, 25, 50, 100, and 150 μm), and external temperature (–10, 10, 30, and 50°C). Through monitoring the temperature change affected by the joule and reaction heats for each case, we suggested critical conditions that led to unavoidable thermal runaway. Thus, this model can be a steppingstone in understanding the correlation between internal short circuits and Li dendrites.

Keywords: internal short circuit, Li dendrite, Li-ion battery, simulation, safety

INTRODUCTION

A lithium-ion battery (LIB) is an energy storage device widely used from small portable electronics to large electric vehicles (EVs) and energy storage systems (ESSs). However, there are still safety risks in state-of-the-art LIBs because of flammable liquid electrolytes. To manage this risk systematically, the European Council for Automotive R&D (EUCAR) has already set the hazard level for LIB cells, modules, and packs depending on the failure type (Josefowitz et al., 2005). According to this criterion, severe battery failures such as fire, fracture, and explosion are categorized into levels 5, 6, and 7, respectively. Regardless of many efforts to prevent those serious accidents, various reasons such as BMS malfunctions (Ye et al., 2016; Ren et al., 2017; Wang Z. et al., 2021), external shock (Feng et al., 2015; Wang et al., 2017), and high temperature exposure (Kim et al., 2007; Feng et al., 2018a) have been reported ceaselessly. Furthermore, since the energy density of advanced LIBs increases, it is not easy to lower the risk of fire or explosion without understanding fundamental reasons at the cell level (Liu et al., 2018; Wang et al., 2019). Among them, an internal short circuit (ISC) must be the most frequently mentioned and highlighted reason for LIB accidents. Unfortunately, the ISC has not been studied systematically and extensively, owing to difficulties in not only detecting the ISC reliably

but also reproducing a similar phenomenon resulting from the same reason. This is why the ISC remains an unconquered research area to date.

To emphasize the severe impact of the ISC in fully charged LIBs, as an example, with an electrochemical model having an LIB electrode pair (loading level = 1.9 mAh cm^{-2} and N/P ratio = 1.1), we could simulate how much current can flow once the Li dendrite with a radius of 5 μm short-circuits the cell. In this simulation, the current density was calculated simply based on Ohm's law without taking both reversible electrode reactions and irreversible side reactions into consideration (Qi et al., 2021). As a result, it is estimated that the current density can increase to 1.97×10^6 mA cm^{-2}, which is about a million times higher than that in a 50-Ah pouch cell at a 1C-rate (1.715 mA cm^{-2}). Thus, a huge amount of IR heat is generated to rapidly increase the temperature near the dendrite inside the battery. In particular, when the internal temperature increases beyond around 100°C, thermal decomposition of the solid electrolyte interphase (SEI) initiates, and subsequent exothermic reactions occur in series (Feng et al., 2018b). Depending on the difference between heat generation and dissipation rates, the temperature can reach the separator collapse limit or not, but once the temperature increases beyond the limit, the direct contact area of the two electrodes gets enlarged, thereby reaching the ignition temperature of organic solvents and resulting in a thermal runaway. In other words, the combination of flammable organic electrolytes as a fuel, exothermal side reactions as a heat source, and the decomposition of lithium transition metal oxide as an oxygen source accelerate the continuous fire or explosion that is hardly extinguished. Due to this high risk of fires or explosion caused by the ISC, many researchers have attempted to clearly understand the causes of the ISC, the mechanisms of heat generation and accumulation, and the temperature rising behavior (Feng et al., 2018b; Zhang et al., 2021).

Among them, many studies have focused on analyzing the temperature rise depending on ISC types, where they can be classified into electrical abuse, internal defects, mechanical abuse, and thermal abuse (Guo et al., 2015; Zhang et al., 2017a; Wang et al., 2019; Foroozan et al., 2020; Zhang et al., 2021). Also, depending on the contact area, ISCs can be divided into the point contact and surface contact (Zhang et al., 2021). Regardless of many previous studies showing threats caused by various types of ISCs, however, it was almost impossible to reproduce or repeat experimental results under the same conditions. Moreover, owing to significantly improved operando analysis methods (Guo et al., 2015; Foroozan et al., 2020), although the size or location of Li dendrites starts to be unveiled in real time, it is still challenging to fabricate model cell systems for dendrite-based ISC studies.

Nonetheless, Zhang et al., (2017a) realized the internal short circuit in a pouch cell using a millimeter-sized shape memory alloy, which shapes a sharp tip at a certain temperature, with high reproducibility. But their model cells could not mimic the small contact area of actual micrometer-sized Li dendrites. Also, the quantities and locations of ISC points were not controlled in their cell systems. In particular, considering the necessity to track some variables such as the internal temperature, local current density and potential, and lithium ion concentrations for better understanding ISCs, various simulations have been attempted with 2D models with micrometer-sized ISCs (Zavalis et al., 2012; Zhang et al., 2017b) or 3D models with millimeter-sized ISCs (Feng et al., 2016; Wang J. et al., 2021). However, as an actual point of view of Li dendrites, 3D models simulating micrometer-sized ISCs are strongly needed to understand the thermal behavior of actual dendrites and to make battery systems under control.

For this purpose, in this study, we built a 3D cell model having various micrometer-sized ISCs in a domain of 1 mm × 1 mm × 0.177 mm. In particular, to secure the reliability of parameters in this model, we primarily constructed a model of a 50 Ah-level NMC442/graphite pouch cell and compared simulated data with measured ones from electrochemical and thermal experiments. First, we simulated the maximum temperatures caused by a single Li dendrite under various external temperatures. Subsequently, while changing both the number of Li dendrites and their distances, the maximum temperature behaviors were also investigated to figure out their interplay. Finally, through analyzing each case study, we estimated the dominant factors to determine the maximum temperatures over time.

MODEL DEVELOPMENTS

Mining Parameters and Building a Model for the 50 Ah-Level Pouch Cell

In order to obtain parameters for developing a reliable 3D ISC model, a 50 Ah-level pouch cell, which has an electrode chemistry of NMC442/graphite and an electrolyte of 1.15 M $LiPF_6$ in ethylene carbonate and ethylmethyl carbonate (EC/EMC = 3/7, v/v) mixture with a size of 247 mm × 227 mm × 8.02 mm, was used (Top in **Figure 1A**). Based on the design parameters of the pouch cell and some literature values on materials, a P2D electrochemical—3D thermal model of the pouch cell was initially built using COMSOL Multiphysics 5.5 (COMSOL Inc., USA) (Bottom of **Figure 1A**; **Supplementary Figure S1**; **Supplementary Table S2**). After that, the initial model was modified better by fitting model parameters through filling the gap between simulated data and experimental ones obtained from the rate capability evaluation [constant current discharging at 0.5, 1, 2, and 5C-rate at 25°C with a 300-A max current cycler (PNE Solution Co., Ltd., Republic of Korea)] (**Figures 1B, C**). In particular, the surface temperature profiles of the 50 Ah-level cell were also obtained through a thermocouple while changing the C-rate. Also, as shown in **Figure 1D**, depending on the C-rate, the model could estimate the surface temperature of the actual pouch cell because not only the heat generation originated from the electrochemical reaction but also the heat dissipation to the surroundings was well simulated in our model. In this simulation, the internal resistance of the tab was not considered because the tab welding conditions of the pouch cell were not accurately known. As shown in **Figure 1D**, the simulation results for the temperature distribution of the pouch cell are locally inaccurate, but it can be seen that at the center of the pouch

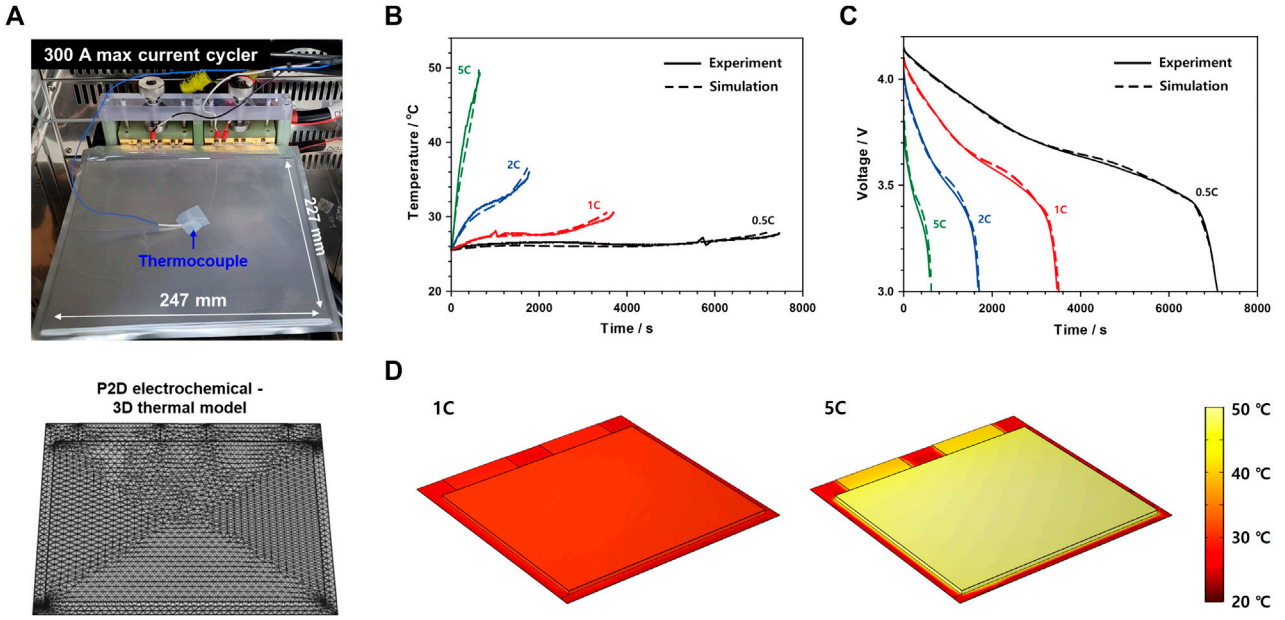

FIGURE 1 | (A) Real image (top) and 3D model structure (bottom) of a 50 Ah-level NMC442/graphite LIB pouch cell. **(B)** Temperature profiles and **(C)** discharge voltage profiles of the pouch cell at various discharge C-rates (0.5, 1, 2, and 5C) along with simulated ones. **(D)** Simulated surface temperatures of the pouch cell in a fully discharged state at different discharge C-rates (1 and 5C).

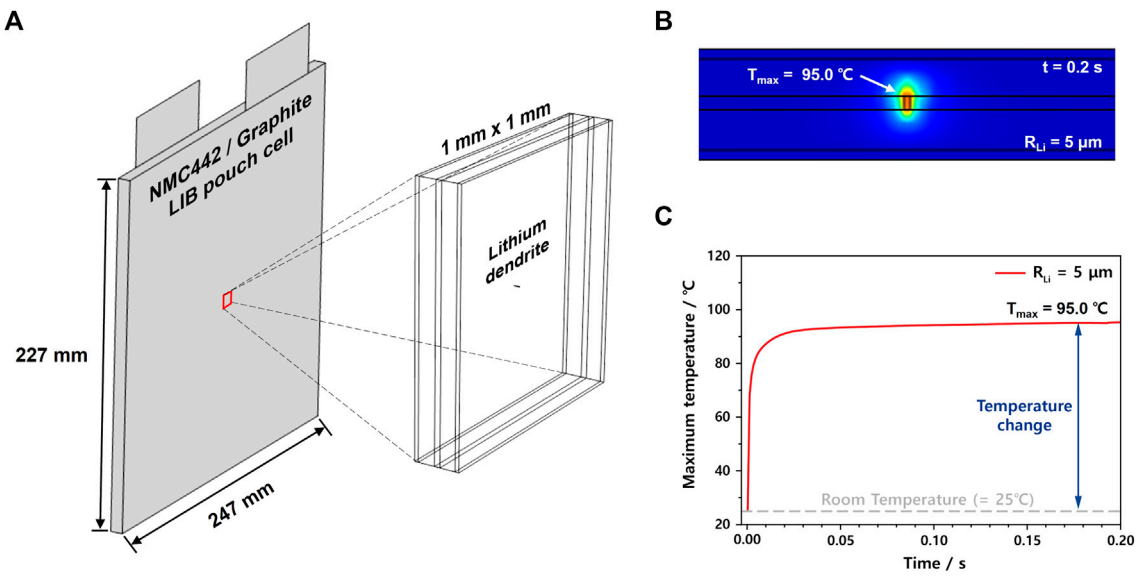

FIGURE 2 | (A) Actual 3D domain size of the ISC model compared to the 50 Ah-level pouch cell. **(B)** Temperature changes in the cross-sectional domain and **(C)** maximum temperature changes with time (from 0 to 0.2 s) of the ISC model having a Li dendrite of a radius of 5 μm.

cell, the temperature increase caused by the electrochemical reaction and the electrode resistance was well calculated. Thus, final model parameters, including the chemical diffusion coefficient and exchange current density, were set in **Supplementary Table S3**, following the aforementioned fitting processes.

3D ISC Model Development

Using the parameters obtained from the cell model (**Supplementary Table S3**), the 3D electrochemical-thermal model for simulating the ISC was developed using COMSOL Multiphysics 5.5. This model is designed to simulate the ISC between two electrodes induced by the formation of

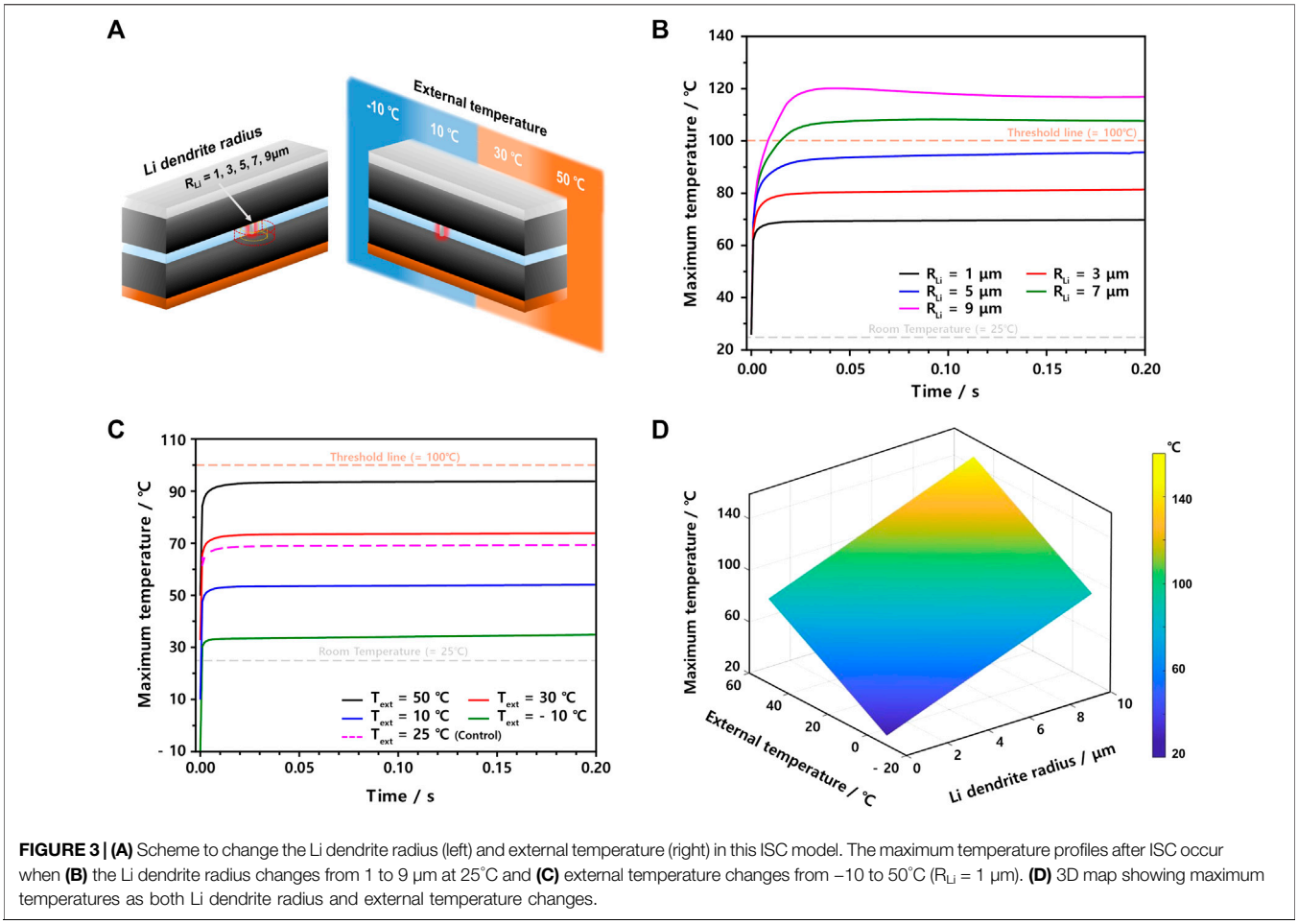

FIGURE 3 | (A) Scheme to change the Li dendrite radius (left) and external temperature (right) in this ISC model. The maximum temperature profiles after ISC occur when **(B)** the Li dendrite radius changes from 1 to 9 μm at 25°C and **(C)** external temperature changes from −10 to 50°C (R_{Li} = 1 μm). **(D)** 3D map showing maximum temperatures as both Li dendrite radius and external temperature changes.

micrometer-sized Li dendrites locally within the pouch cell. Considering both calculation time and sufficiently large domain size compared to Li dendrites, this 3D model was designed in a volume of 1 mm × 1 mm × 0.177 mm with the same parameters and boundary conditions as the entire pouch cell. Furthermore, considering the excellent thermal conductivity and heat capacity of the current collector and the larger value of in-plane thermal conductivity of the electrode layer than through-plane (Zhang et al., 2020) thermal conductivity, we did not have to consider thermal transfer from any layer to the peripheral layer (**Figure 2A**). As described in the middle of the 3D model, the cylindrical Li dendrite with a radius of 5 μm looks like just a thin line in the simulated domain. This is because Li dendrites are known to be grown through the pores in the separator as cylindrical shapes rather than fractals, which can be readily formed in the liquid electrolyte under no physical barriers (Jana et al., 2015; Mu et al., 2019; Jungjohann et al., 2021).For convenience, in this work, the shape of Li dendrites was assumed to be a cylinder having the same height as the separator thickness. The range of the Li dendrite radius was initially controlled from 1 to 5 μm based on previous works showing actual Li dendrite sizes (Frenck et al., 2019; Guo et al., 2020; Liu et al., 2020) and then increased to 9 μm to simulate catastrophic situations. This model can simulate the thermal behavior only caused by the current flow through the Li dendrite, where the corresponding current value is dependent on the amount and state of active materials in both electrodes. In other words, this model does not consider the thermal behavior related to side reactions such as SEI breakdown, separator melting, or active material decomposition. Thus, for instance, we can estimate temperature changes around Li dendrites, as shown in **Figure 2B**, or maximum temperature changes as a function of time, as shown in **Figure 2C**.

RESULTS AND DISCUSSION

To systematically investigate the effects of Li dendrites on temperature changes in internal short-circuited LIB cells, we utilized our 3D ISC model while changing the Li dendrite radius from 1 to 9 μm and the external temperature from −10 to 50°C (**Figure 3A**). In the case of the Li dendrite radius study, the external temperature was set to 25°C. As depicted in **Figure 3B**, the radius of the Li dendrite governs the maximum temperature. In more detail, when the radius is as small as 1 μm, the temperature just increases to 69°C within 0.03 s. On the other hand, when the radius becomes greater than or equal to 7 μm, the maximum temperature passes a threshold point of around 100°C, where SEI begins to be decomposed. In particular, as soon as the ISC

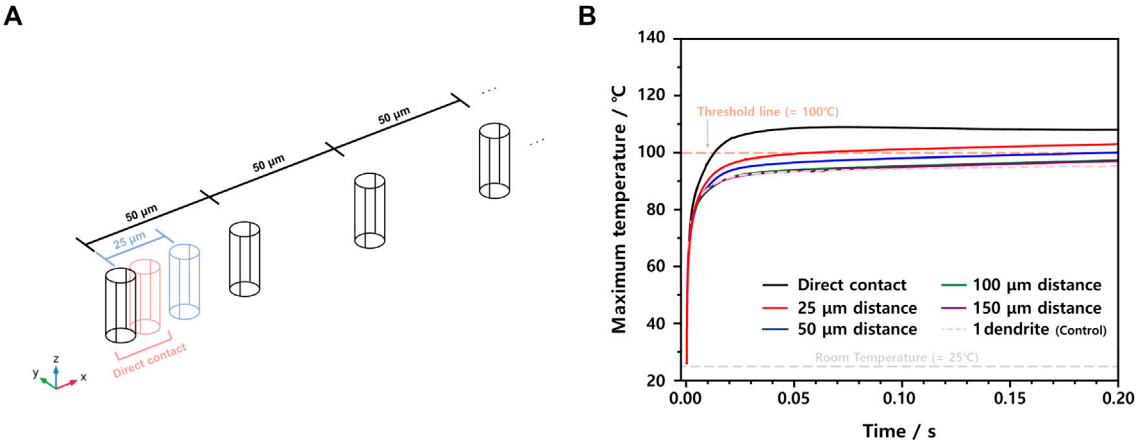

FIGURE 4 | (A) Scheme describing the relative distance of two Li dendrites of 5 μm radius and **(B)** maximum temperature profiles of ISC models depending on the distance of 10 μm (direct contact), 25, 50, 100, and 150 μm.

occurs, the temperature rapidly increases to a saturated value within 0.03 s for all cases because a huge current flows within a very short period as the adiabatic condition. However, when the amount of heat transfer becomes almost the same as that of joule heating, the maximum temperature is maintained at its specific point regardless of the Li dendrite radius. When the effect of the external temperatures on the maximum temperature was also simulated while fixing the Li dendrite radius to 1 μm, as shown in **Figure 3C**, the maximum temperature changed similarly, as in **Figure 3B**. However, although the maximum temperature is strongly dependent on the external temperature, the temperature difference before and after the ISC seems quite similar at around 44°C. Specifically, in this case, when the external temperature is greater than or equal to 50°C, the maximum temperature passes the first threshold point, just like the case of the Li dendrite radius of 7 μm. Similar to this analysis, we need to check both the Li dendrite radius and external temperature simultaneously, as shown in **Figure 3D**, where safe and dangerous regions are colored by the combination of blue and yellow with different ratios. Thus, our ISC model can provide us with a platform to understand the impact of the Li dendrite size and external temperature on the thermal runaway of LIB cells.

As the next step, we need to consider some ISC situations having more than a single Li dendrite by designing their relative distances, as in **Figure 4A**, where the base distance of 50 μm is set by assuming that another Li dendrite of a radius of 5 μm can exist ten times farther away. Also, although the probability is low, two Li dendrites that are contacted or located nearby are also considered. Based on the simulated data summarized in **Figure 4B**, when the distance between two Li dendrites is sufficiently far, e.g., 100 μm, the maximum temperatures in two Li dendrites cases are almost the same as those in a single Li dendrite one. In the region of less than 100 μm distance, of course, the maximum temperature tends to increase as the distance becomes shorter. However, even in the direct contact case, the maximum temperature additionally increased by 12.7°C to be 107.7°C while 95.0°C was reached in the reference single Li dendrite case (**Supplementary Table S4**). Thus, when more than one Li dendrite is formed simultaneously, the risk of thermal runaway of LIBs does not increase proportionally. In other words, when Li dendrites are formed relatively far away enough not to interplay, the probability of encountering catastrophic events becomes lower.

To confirm the effect of the distance between Li dendrites on the maximum temperature, we simulated the thermal behaviors of two ISC models: one has a big Li dendrite of 3 μm radius, and the other has nine small Li dendrites of 1 μm radius, where they are located by 200 μm, while their total areas are identical to be 9π μm^2 (**Figures 5A,B**). As readily estimated from the results in **Figures 3**, **4**, the maximum temperature is mainly governed by the radius of the Li dendrite regardless of Li dendrite numbers only if each dendrite is far away. However, as observed in **Figure 5C**, the maximum temperature of nine small Li dendrites tends to gradually increase with time, thereby reaching a little higher value of around 4°C after 0.20 s. This continuous increase can be ascribed to the average temperature of 29.9°C, which is even higher than the single big Li dendrite case (**Figure 5D**; **Supplementary Table S5**). In other words, when there are many heat sources, the heat dissipation rate reduces with time, and both the maximum and average temperature increase steadily.

To investigate the influence of the Li dendrite (R_{Li} = 5 μm) number on the maximum temperature in more detail, we built four ISC models having one, three, five, and nine Li dendrites with 200 μm distances, as shown in **Figure 6A**, where the temperature distribution of each case is expressed through different colors at 0.2 s after ISC occurs. As already observed in **Figures 4**, **5**, the maximum temperature in the initial state, e.g.,t = 0.03 s, is not dependent on the number of Li dendrites. However, the temperature increase rate is largely affected by the Li dendrite number, as shown in **Figure 6B**. More specifically, while the ISC model with one Li dendrite reaches the maximum temperature of 95.0°C at 0.2 s, the maximum temperatures of five and nine Li dendrite models exceed the critical temperature of 100°C, i.e., 101.6 and 109.0°C, respectively (**Supplementary Table**

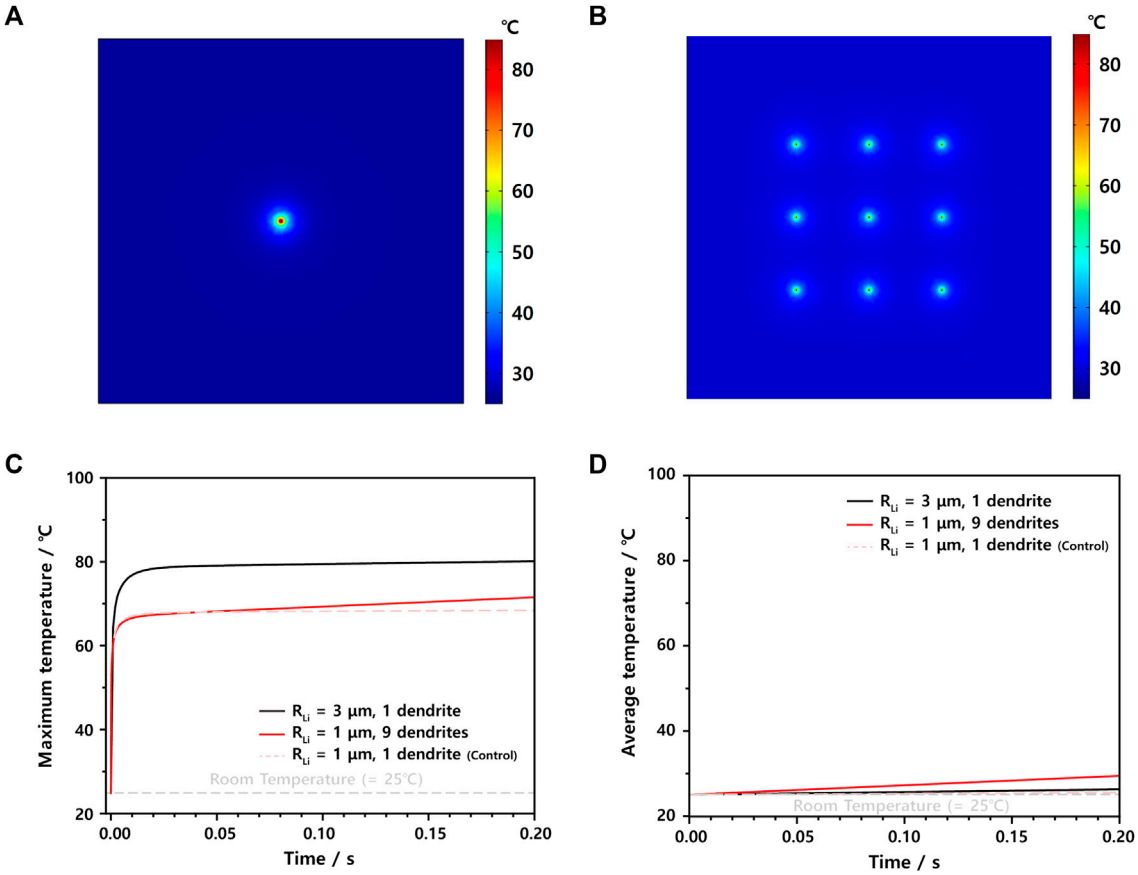

FIGURE 5 | Thermal 2D color maps at 0.2 s of ISC models having **(A)** one large Li dendrite of 3 μm radius and **(B)** nine small Li dendrites of 1 μm radius. **(C)** Maximum temperature profiles and **(D)** average temperature profiles of the aforementioned two ISC models, with the control case having one small Li dendrite of 1 μm.

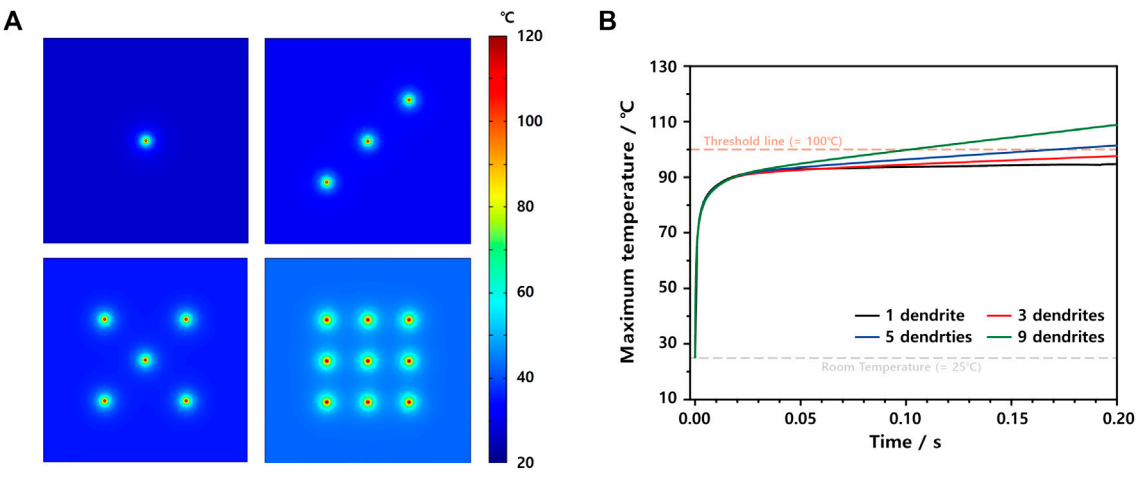

FIGURE 6 | (A) Thermal 2D color map at 0.2 s of ISC models having one Li dendrite, three Li dendrites, five Li dendrites, and nine Li dendrites. **(B)** Maximum temperature profiles of ISC models depending on the number of Li dendrites.

S6). Thus, the maximum temperature in the initial state is mainly dependent on the Li dendrite size, but the number of Li dendrites significantly affects the temperature increase rate. With this ISC model, we can provide a good platform to investigate the influence of Li dendrite sizes and distribution on the thermal behaviors of LIB cells in 3D domains.

CONCLUSION

We developed a 3D electrochemical–thermal model to simulate the ISC caused by the Li dendrites, which considers external temperature, Li dendrite size, number, and relative distances simultaneously. With assumptions such as no side reactions and a simplified Li dendrite shape, the maximum temperature at the start point (0 s) is determined by the external temperature, and within a short period (from 0 to 0.03 s), the maximum temperature increase is governed by the size of the Li dendrite. After a steep temperature increase (after 0.03 s), the maximum temperature is affected by the number of Li dendrites. Therefore, these conditions affecting the thermal behaviors of the LIB cell should be considered simultaneously. Additionally, using our model, the relative distance effect of Li dendrites was investigated. The Li dendrites did not affect each other's maximum temperature rise when they were sufficiently far away. This result shows that even if many Li dendrites are generated simultaneously, the risk of thermal runaway does not increase unconditionally.

Based on this advanced analysis using a 3D ISC model, the limitation of dendrite-based ISC evaluation, which is almost impossible to obtain experimental reproducibility , was addressed, and governing factors for maximum temperature behavior over time were determined. We believe that our model can provide additional insights on the correlation between dendrite-based ISCs and thermal behavior of LIB cells, which can be the basis for further investigating and understanding the thermal runaway.

DATA AVAILABILITY STATEMENT

The original contributions presented in the study are included in the article/**Supplementary Material**, further inquiries can be directed to the corresponding authors.

AUTHOR CONTRIBUTIONS

SK: formal analysis, investigation, methodology, software, conceptualization, data curation, and writing—original draft. JS: conceptualization, investigation, methodology, and software. HL: investigation. SJ: investigation. JP: investigation. HL: conceptualization and methodology. YL: supervision, conceptualization, methodology, formal analysis, and writing—review and editing.

FUNDING

This work was supported by the National Research Foundation of Korea (NRF) grant funded by the Korean government (MSIT) (No. 2020R1A4A4079810) and the Electronics and Telecommunications Research Institute (ETRI) grant funded by the Korean government (20ZB1200, Development of ICT Materials, Components, and Equipment Technologies).

ACKNOWLEDGMENTS

We are also very grateful for the support from the DGIST Supercomputing and Big Data Center.

SUPPLEMENTARY MATERIAL

The Supplementary Material for this article can be found online at: https://www.frontiersin.org/articles/10.3389/fmats.2022.850610/full#supplementary-material

REFERENCES

Feng, X., He, X., Ouyang, M., Wang, L., Lu, L., Ren, D., et al. (2018a). A Coupled Electrochemical-Thermal Failure Model for Predicting the Thermal Runaway Behavior of Lithium-Ion Batteries. *J. Electrochem. Soc.* 165, A3748–A3765. doi:10.1149/2.0311816jes

Feng, X., Ouyang, M., Liu, X., Lu, L., Xia, Y., and He, X. (2018b). Thermal Runaway Mechanism of Lithium Ion Battery for Electric Vehicles: A Review. *Energ. Storage Mater.* 10, 246–267. doi:10.1016/j.ensm.2017.05.013

Feng, X., Sun, J., Ouyang, M., Wang, F., He, X., Lu, L., et al. (2015). Characterization of Penetration Induced thermal Runaway Propagation Process within a Large Format Lithium Ion Battery Module. *J. Power Sourc.* 275, 261–273. doi:10.1016/j.jpowsour.2014.11.017

Feng, X., Weng, C., Ouyang, M., and Sun, J. (2016). Online Internal Short Circuit Detection for a Large Format Lithium Ion Battery. *Appl. Energ.* 161, 168–180. doi:10.1016/j.apenergy.2015.10.019

Foroozan, T., Sharifi-Asl, S., and Shahbazian-Yassar, R. (2020). Mechanistic Understanding of Li Dendrites Growth by in- Situ/operando Imaging Techniques. *J. Power Sourc.* 461, 228135. doi:10.1016/j.jpowsour.2020.228135

Frenck, L., Sethi, G. K., Maslyn, J. A., and Balsara, N. P. (2019). Factors that Control the Formation of Dendrites and Other Morphologies on Lithium Metal Anodes. *Front. Energ. Res.* 7. doi:10.3389/fenrg.2019.00115

Guo, S., Wang, L., Jin, Y., Piao, N., Chen, Z., Tian, G., et al. (2020). A Polymeric Composite Protective Layer for Stable Li Metal Anodes. *Nano Convergence* 7, 21. doi:10.1186/s40580-020-00231-w

Guo, Z., Zhu, J., Feng, J., and Du, S. (2015). Direct *In Situ* Observation and Explanation of Lithium Dendrite of Commercial Graphite Electrodes. *RSC Adv.* 5, 69514–69521. doi:10.1039/c5ra13289d

Jana, A., Ely, D. R., and García, R. E. (2015). Dendrite-separator Interactions in Lithium-Based Batteries. *J. Power Sourc.* 275, 912–921. doi:10.1016/j.jpowsour.2014.11.056

Josefowitz, W., Kranz, H., Macerata, D., Soczka-Guth, T., Mettlach, H., Porcellato, D., et al. (2005). "Assessment and Testing of Advanced Energy Storage Systems for Propulsion–European Testing Report," in Proceedings of the 21 worldwide battery, hybrid and fuel cell electric vehicle symposium & exhibition. Monte Carlo, Monaco: EVS21 Organization, 2–6.

Jungjohann, K. L., Gannon, R. N., Goriparti, S., Randolph, S. J., Merrill, L. C., Johnson, D. C., et al. (2021). Cryogenic Laser Ablation Reveals Short-Circuit Mechanism in Lithium Metal Batteries. *ACS Energ. Lett.* 6, 2138–2144. doi:10.1021/acsenergylett.1c00509

Kim, G.-H., Pesaran, A., and Spotnitz, R. (2007). A Three-Dimensional thermal Abuse Model for Lithium-Ion Cells. *J. Power Sourc.* 170, 476–489. doi:10.1016/j.jpowsour.2007.04.018

Liu, K., Liu, Y., Lin, D., Pei, A., and Cui, Y. (2018). Materials for Lithium-Ion Battery Safety. *Sci. Adv.* 4, eaas9820. doi:10.1126/sciadv.aas9820

Liu, L., Feng, X., Zhang, M., Lu, L., Han, X., He, X., et al. (2020). Comparative Study on Substitute Triggering Approaches for Internal Short Circuit in Lithium-Ion Batteries. *Appl. Energ.* 259, 114143. doi:10.1016/j.apenergy.2019.114143

Mu, W., Liu, X., Wen, Z., and Liu, L. (2019). Numerical Simulation of the Factors Affecting the Growth of Lithium Dendrites. *J. Energ. Storage* 26, 100921. doi:10.1016/j.est.2019.100921

Qi, X., Liu, B., Pang, J., Yun, F., Wang, R., Cui, Y., et al. (2021). Unveiling Micro Internal Short Circuit Mechanism in a 60 Ah High-Energy-Density Li-Ion Pouch Cell. *Nano Energy* 84, 105908. doi:10.1016/j.nanoen.2021.105908

Ren, D., Feng, X., Lu, L., Ouyang, M., Zheng, S., Li, J., et al. (2017). An Electrochemical-thermal Coupled overcharge-to-thermal-runaway Model for Lithium Ion Battery. *J. Power Sourc.* 364, 328–340. doi:10.1016/j.jpowsour.2017.08.035

Wang, H., Lara-Curzio, E., Rule, E. T., and Winchester, C. S. (2017). Mechanical Abuse Simulation and thermal Runaway Risks of Large-Format Li-Ion Batteries. *J. Power Sourc.* 342, 913–920. doi:10.1016/j.jpowsour.2016.12.111

Wang, J., Mei, W., Cui, Z., Dong, D., Shen, W., Hong, J., et al. (2021a). Investigation of the thermal Performance in Lithium-Ion Cells during Polyformaldehyde Nail Penetration. *J. Therm. Anal. Calorim.* 145, 3255–3268. doi:10.1007/s10973-020-09853-y

Wang, Q., Mao, B., Stoliarov, S. I., and Sun, J. (2019). A Review of Lithium Ion Battery Failure Mechanisms and Fire Prevention Strategies. *Prog. Energ. Combustion Sci.* 73, 95–131. doi:10.1016/j.pecs.2019.03.002

Wang, Z., Yuan, J., Zhu, X., Wang, H., Huang, L., Wang, Y., et al. (2021b). Overcharge-to-thermal-runaway Behavior and Safety Assessment of Commercial Lithium-Ion Cells with Different Cathode Materials: A Comparison Study. *J. Energ. Chem.* 55, 484–498. doi:10.1016/j.jechem.2020.07.028

Ye, J., Chen, H., Wang, Q., Huang, P., Sun, J., and Lo, S. (2016). Thermal Behavior and Failure Mechanism of Lithium Ion Cells during Overcharge under Adiabatic Conditions. *Appl. Energ.* 182, 464–474. doi:10.1016/j.apenergy.2016.08.124

Zavalis, T. G., Behm, M., and Lindbergh, G. (2012). Investigation of Short-Circuit Scenarios in a Lithium-Ion Battery Cell. *J. Electrochem. Soc.* 159, A848–A859. doi:10.1149/2.096206jes

Zhang, G., Wei, X., Tang, X., Zhu, J., Chen, S., and Dai, H. (2021). Internal Short Circuit Mechanisms, Experimental Approaches and Detection Methods of Lithium-Ion Batteries for Electric Vehicles: A Review. *Renew. Sustain. Energ. Rev.* 141, 110790. doi:10.1016/j.rser.2021.110790

Zhang, L., Zhao, P., Xu, M., and Wang, X. (2020). Computational Identification of the Safety Regime of Li-Ion Battery Thermal Runaway. *Appl. Energy* 261, 114440.

Zhang, M., Du, J., Liu, L., Stefanopoulou, A., Siegel, J., Lu, L., et al. (2017a). Internal Short Circuit Trigger Method for Lithium-Ion Battery Based on Shape Memory Alloy. *J. Electrochem. Soc.* 164, A3038–A3044. doi:10.1149/2.0731713jes

Zhang, M., Liu, L., Stefanopoulou, A., Siegel, J., Lu, L., He, X., et al. (2017b). Fusing Phenomenon of Lithium-Ion Battery Internal Short Circuit. *J. Electrochem. Soc.* 164, A2738–A2745. doi:10.1149/2.1721712jes

Conflict of Interest: The authors declare that the research was conducted in the absence of any commercial or financial relationships that could be construed as a potential conflict of interest.